WORDS (manuscript, Tables, Figures and Scheme):7980

Tunable copper-hydrotalcite derived mixed oxides for sustainable ethanol condensation to *n*-butanol in liquid phase

Patricia Benito[a*], Angelo Vaccari[a], Claudia Antonetti[b], Domenico Licursi[b], Nicola Schiarioli[a], Enrique Rodriguez-Castellón[c], Anna Maria Raspolli Galletti[b]*

[a]Dipartimento di Chimica Industriale "Toso Montanari", Università di Bologna, Viale Risorgimento 4, 40136, Bologna, Italy.

[b]Dipartimento di Chimica e Chimica Industriale, Università di Pisa, Via G. Moruzzi 13, 56124 Pisa, Italy.

[c]Departamento de Química Inorgánica, Universidad de Málaga, 29071 Málaga, Spain

Abstract

Improvement of processes starting from renewable feedstocks to produce chemicals and biofuels up to now derived from fossil carbon feedstocks is paramount to creating environmentally sustainable industrial processes. Guerbet condensation of ethanol to give *n*-butanol represents a turning point not only respect to the traditional petrochemical "oxo" process, but also to the bio-chemical path (Acetone Butanol Ethanol "ABE" process). In this work, different Cu/Mg/Al hydrotalcite-derived mixed oxides catalysts, with Cu atomic content in the range 7.6-1.0 %, were synthetised, characterized, and tested for the Guerbet reaction. The adopted catalysts are easy to produce, and based on available, cheap and non-toxic metals. Tailoring Cu-content in hydrotalcite-derived Cu/Mg/Al mixed oxides allowed us to selectively address this reaction towards *n*-butanol formation, highlighting how a low Cu-content favours the condensation to *n*-butanol and higher alcohols, in particular *n*-hexanol, decreasing the ester formation. The Guerbet selective co-production of [*n*-butanol + *n*-hexanol] is economically even more attractive than that of the sole *n*-butanol, being both saleable products. Good catalytic performances to *n*-butanol and *n*-hexanol were achieved, in a batch process carried out under subcritical conditions. These catalysts have

List of abbreviations: Ethanol (EtOH); *n*-Butanol (BuOH); Ethyl acetate (AcOEt); Hexanol (HexOH); Methanol (MeOH); *n*-Propanol (PrOH); Hydrotalcite-type (HT); Cu/Mg/Al HT-derived mixed oxides (Cu-HT); X-ray diffraction (XRD); Specific surface area (SSA); Temperature programmed reduction by H_2 (H_2-TPR); Thermal conductivity detector (TCD); Temperature programmed desorption of CO_2 (CO_2-TPD); High resolution transmission electron microscopy (HRTEM); Energy dispersive X-ray spectrometry (EDS); X-ray photoelectron spectroscopy (XPS); Inductive coupled plasma spectroscopy (ICPS); Gas chromatograph coupled with flame-ionization detector (GC-FID); Gas chromatography – mass spectrometry (GC-MS); Yield (Y); Selectivity (Sel.); Conversion (Conv.); Space time yield (STY); Scanning transmission electron microscopy coupled with high angle annular dark field detector (HAADF/STEM).

required a simple procedure of recovery, showing good recyclability, in term of catalytic performances to give the target products, thus opening the way to applicative perspectives.

Keywords: Guerbet reaction; alcohol coupling; ethanol condensation; *n*-butanol; copper-hydrotalcite.

*Corresponding authors, e-mail: patricia.benito3@unibo.it; anna.maria.raspolli.galletti@unipi.it.

1. Introduction

Alcohol condensations have attracted high interest in the last few years because of both environmental concerns and the new economic opportunities seen in bio-based feedstocks. In this context, a great interest is focused on the ethanol (EtOH) dimerization to give *n*-butanol (BuOH), also known as Guerbet reaction (Wu et al., 2018; Zhang et al., 2016). EtOH is one of the most important bio-platform molecules, having many applications as bio-fuel, solvent, and as starting material to produce different added-value chemicals (Machado et al., 2018). BuOH is of particular interest for the production of acrylic acid/esters (Marcu et al., 2013), as solvent and as fuel additive, being considered a valuable alternative to EtOH (Hashim et al., 2017). Currently, BuOH is produced from fossil resources by propylene hydroformylation/hydrogenation. On the other hand, the use of renewable feedstocks for BuOH production has become achievable, though, either by direct fermentation of carbohydrates to yield BuOH (e.g., the Acetone-Butanol-Ethanol "ABE" process), or by Guerbet coupling reaction. Regarding the first bio-route, which occurs through fermentation of sugar, glycerol, or lignocellulosic feedstocks, it has still many unsolved drawbacks, such as bio-chemical limitations, low BuOH yield, high substrate cost (Jafari et al., 2017; Pereira et al., 2015). Moreover, many technological limits, including the energy-intensive distillation, due to the low final BuOH concentration, and wastewater post-treatments, cause the poor economics of this route. A very recent techno-economic analysis of the Guerbet reaction has confirmed its feasibility on an industrial scale (Nezam et al., 2019) and life cycle analysis of Guerbet process suggests that it would result in a nontrivial (~50%-80 %) reduction in greenhouse gas emissions when tuned for diesel production (Sreekumar et al., 2015).

Guerbet approach involves the condensation of two molecules of alcohols to give a β-alkylated dimer alcohol, with the concomitant release of water. This condensation reaction is generally reported to proceed by five successive steps (Scheme 1): 1) dehydrogenation of the starting alcohols

to give the corresponding aldehydes; 2) aldol condensation of the aldehydes; 3) dehydration; and 4-5) final hydrogenations of the unsaturated aldol condensation products to give the higher Guerbet alcohols (Gabriëls et al., 2015).

Scheme 1, near here

The dehydrogenation (Step 1) is endothermic, thermodynamically favored at high temperatures, and often reported as the rate limiting step, in particular when lower alcohols are employed as substrates in the liquid phase (Dowson et al., 2013). In order to improve both the dehydrogenation and the successive hydrogenation steps, the presence of a transition metal in the catalytic system can be crucial. On the other hand, the aldol condensation (Step 2) is catalyzed by basic, acidic or amphoteric catalysts, and is thermodynamically unfavorable, whilst the successive aldol dehydration to give the α,β-unsaturated aldehyde (Step 3) is highly favorable and shifts the overall reaction towards the desired products. Many authors have reported the negative effect of the co-produced water on the reaction behavior, in particular working in the liquid phase (Marcu et al., 2009; Riittonen et al., 2014). Finally, the hydrogenation reactions (Steps 4 and 5) are favored by low temperatures. Considering all the involved reactions, it is remarkable that the adopted catalytic system and reaction conditions play a key role for obtaining BuOH. The above mechanism is largely accepted as the effective one at low temperatures (in particular in the liquid phase) and in the presence of hydrogenating/dehydrogenating catalytic components. For the Guerbet condensation of EtOH to BuOH in the presence of purely basic heterogeneous catalysts, performed in the gas phase above 400 °C, also direct condensation mechanisms have been proposed (Chieregato et al., 2015). The Guerbet reaction to give isobutanol starting from mixtures of methanol (MeOH) and *n*-propanol (PrOH), was studied using Cu chromite in the presence of basic Mg-Al mixed oxides derived from hydrotalcite-type (HT) precursors (Carlini et al., 2004) or Cu/Mg/Al mixed oxide catalysts obtained from HT precursors (Carlini et al., 2005). These last systems resulted active and selective towards the Guerbet alcohol formation not only in liquid but also in gas phase at 280 °C, reaching selectivity around 80 mol %, at complete propanol conversion. The use of HT-derived mixed oxides was also reported for EtOH condensation both in liquid and in gas phase. These mixed oxides were used as $MgAlO_x$ (Carvalho et al., 2012; Di Cosimo et al., 1998, 2000; León et al., 2011) or as metal-promoted catalysts (Hosoglu et al., 2015; Marcu et al., 2009, 2013). The addition of Cu significantly increased the dehydrogenating activity to acetaldehyde, reducing the amount of ethylene formed by dehydration at temperature > 300°C (Hosoglu et al., 2015). Marcu et al. (2009) studied the valorization of EtOH over Cu/Mg/Al mixed oxides obtained from HT precursors by calcination, performing the condensation at 200-250 °C. The conversion was always

lower than 10 mol %, and an optimum yield to BuOH was ascertained for Cu content in the mixed oxides between 5 and 10 wt%. The same authors also studied the effect of different cations in Me/Mg/Al systems (Me = Pd, Ag, Mn, Fe, Cu, Sm or Yb), reporting good performances with the Pd-containing mixed oxide (Marcu et al., 2013). A strict correlation between the amount of basic sites of medium and high strength and the selectivity to BuOH was evidenced, the presence of significant amount of acid sites increasing the selectivity to acetaldehyde and its acetal 1,1-diethoxyethane. The role of acid-base properties in the Guerbet reaction has been recently well-evidenced also for MgAl-HT derived oxides with different Mg/Al ratios (Li, X.N. et al., 2018). The highest conversion was found for materials with the highest number of basic and acid sites. If the positive effect of basic sites was expected, the positive role of a certain acidity was related to the catalytic effect on aldol reaction and aldol dehydration. Recently pre-reduced Ni/Mg/Al HT-derived mixed oxides were tested in flow reactor and EtOH conversion increased linearly from 7 to 22 mol% when the temperature was increased from 200 to 275 °C, the selectivity to BuOH remaining around 50 mol % (Pang et al., 2016). Interesting performances in EtOH condensation were also ascertained in supercritical conditions at 310 °C and 80 atmospheres using Ni/Cu/Mg/Al HT-derived mixed oxides, although under these harsh reaction conditions the C-balance was around 75 %, due to the formation of volatile by-products. On the other hand, when the same catalysts were adopted at 220 °C in the liquid phase, better C-balance but much lower catalytic performances were ascertained (Sun et al., 2017). In summary, up to now, heterogeneous systems able to afford good catalytic performances working in liquid phase at temperatures lower than the EtOH critical one have not been definitely developed. In particular, the selectivity of the catalyst towards BuOH (or to BuOH + HexOH) formation must be improved thus making the reaction applicable in a sustainable chemical and/or fuel industry (Nezam et al., 2019). In this work, Guerbet reaction was studied employing *ad hoc* synthesized Cu/Mg/Al HT-derived mixed oxides (Cu-HT) of different composition, in order to relate the catalytic performances with their main properties, which can be properly tuned for the optimal BuOH production.

2. Materials and Methods

2.1 Materials

EtOH (Aldrich) was dried by distillation under dry argon after refluxing for 6 h on magnesium methoxide. Cu-HT precursors were prepared by coprecipitation at constant pH; a 2 M solution containing $Cu(NO_3)_2 \cdot 2.5H_2O$, $Mg(NO_3)_2 \cdot 6H_2O$ and $Al(NO_3)_3 \cdot 9H_2O$ in the appropriate ratios was slowly added to a 1 M solution containing Na_2CO_3 and NaOH. The atomic ratios percent (a.r.%)

used in this work were: Cu/Mg/Al = 7.6/62.7/29.7, 2.8/68.2/29.0, and 1.0/69.0/30.0. The pH was kept constant (10.5 ± 0.2) by dropwise NaOH addition. The obtained precipitate was kept in suspension under stirring at 60 °C for 45 min, then filtered and washed with distilled water until a Na_2O content lower than 0.02 wt.% was obtained. The precipitate was dried overnight at 60 °C and calcined at 500 °C for 7 h. The samples were labelled Cu7.6, Cu2.8 and Cu1.0, indicating the Cu a.r. A commercial Mg/Al hydrotalcite MG Puralox 79/390 was purchased by Sasol (MgO: 74.0 wt %, Al_2O_3: 26.0 wt %), calcined at 500 °C for 7 h, and stored under dry argon.

2.2 Catalyst characterization

The X-ray diffraction (XRD) analysis of the powders was carried out using a PANalytical X'Pert diffractometer equipped with a copper anode (λmean = 0.15418 nm) and a fast X'Celerator detector. Wide-angle diffractogram was collected over 2θ range from 5 to 70° with a step size of 0.05° and counting time 15 s.

Specific surface area (SSA) assessment was carried out using a Micromeritics ASAP 2020 instrument; samples were heated up to 150 °C and evacuated at a pressure better than 0.02 Torr, and kept for 150 min at this temperature.

Temperature programmed reduction by H_2 (H_2-TPR) was performed in an AutoChem II apparatus (Micromeritics) with pelletized catalysts. The catalyst was firstly cleaned at 150 °C under 30 mL/min He flow for 30 min. After cooling to 50 °C, the carrier gas was switched to 5 % H_2/Ar (v/v) at 30 mL/min. When the baseline was stable, the temperature was increased up to 800 °C with a heating rate of 10 °C/min, while the amount of H_2 consumed was measured by means of a thermal conductivity detector (TCD).

Temperature programmed desorption of CO_2 (CO_2-TPD) experiments were performed in an Autochem II (Micromeritics) instrument with powdered catalysts. The sample was placed in a quartz tubular reactor and pretreated at 500 °C under 30 mL/min He flow for 120 min, then cooled down to 40 °C and exposed to 10 % CO_2/He (v/v) stream with a flow rate of 30 mL/min for 2 h. The physisorbed CO_2 was removed by He purging (30 mL/min) for 60 min. Then, the sample was heated at 10 °C/min up to 800 °C and the desorbed CO_2 was monitored and recorded using an online Mass spectrometer (Cirrus 2, MKS instruments) which was calibrated by manual injections of pure CO_2 (m/z = 44) pulses.

A blank test flowing only Ar showed no CO_2 desorption in the 30-500 °C range investigated, while H_2O and CO_2 evolved above 500 °C, namely at higher temperatures than that for calcination,

indicating the not total dehydroxilation and decarbonation of the samples, thus the range analyzed for studying the basicity of the samples was 40-500 °C.

High resolution transmission electron microscopy (HRTEM) characterization was carried out by a TEM/STEM FEI TECNAI F20 microscope, equipped with an Energy Dispersive X-ray Spectrometry (EDS) analyzer. Powder catalysts were suspended in EtOH under ultrasounds for 20 min. The suspension was subsequently deposited on an Au grid with lacey multi-foil carbon film and dried at 100 °C before doing the measurement.

X-Ray Photoelectron Spectroscopy (XPS) data were collected using a Physical Electronics PHI 5700 spectrometer with non-monochromatic Mg-Kα radiation (300 W, 15 kV, 1253.6 eV) for the analysis of the core level signals of the studied elements and with a multichannel detector. Spectra of powdered samples were recorded with a constant pass energy value of 29.35 eV, using a 720 μm diameter analysis area. Under these conditions, the Au $4f_{7/2}$ line was recorded with 1.16 eV FWHM at a binding energy of 84.0 eV. The spectrometer energy scale was calibrated using Cu $2p_{3/2}$, Ag $3d_{5/2}$, and Au $4f_{7/2}$ photoelectron lines at 932.7, 368.3, and 84.0 eV, respectively. The Cu 2p and C 1s core level spectra were first recorded with a short irradiation time of 10 min to avoid, as much as possible, photoreduction of Cu^{2+}. The PHI ACCESS ESCA-V6.F software package was used for acquisition and data analysis. The recorded spectra were always fitted using Gauss–Lorentz curves, in order to determine the binding energy of the different elements core levels more accurately.

The copper content of the employed catalysts Cu7.6, Cu2.8 and Cu1.0 was determined by Inductive Coupled Plasma Spectroscopy (ICPS) using a Jobin-Yvon JY 2000 Analizer. The samples were weighed into Teflon bombs followed by addition of acid mixture. Thereafter, microwave oven (MARS) was applied in the digestion and appropriate dilutions were performed prior to the ICPS analysis. Microwave digestion was carried out in a CEM microwave accelerated reaction system MARS 6.

2.3 Catalytic reactions

The Guerbet condensation of EtOH was carried out in a batch reaction system, using a 300 ml Parr autoclave, with a mechanical stirrer and a heating system controlled by means of a Parr controller 4848. The proper amount of solid catalyst was introduced in the reactor under dry argon, then this was evacuated and 893 mmol of EtOH (52.12 ml) with 350 μl of benzene as internal standard were added through the sampling valve. The reactor was subsequently pressurized with N_2 (4 MPa), and heated at the reaction temperature (215 or 230 °C).

Regarding the recyclability study, the Cu1.0 catalyst was re-used under the same reaction conditions of the first cycle. The recycled catalyst was tested: i) after EtOH washing and successive calcination at 500 °C for 7 h; ii) after EtOH washing and drying up to constant weight.

When the catalyst was beforehand pre-reduced, the proper amount of heterogeneous catalyst and 60 ml of MeOH were introduced in the reactor as described above, the autoclave was pressurized with H_2 up to 5 MPa and heated at 180 °C for 5 h for the metal component pre reduction. Then the reactor was evacuated, MeOH was removed under vacuum and then EtOH was introduced by suction. The reactor was subsequently pressurized with N_2 (4 MPa) and heated at the chosen temperature.

All the condensation experiments were carried out in duplicate and the composition of the reaction mixtures resulted reproducible to within ±5%.

The reaction profile was followed by collecting at different times little portions of the reaction mixture through the sample valve and quickly cooling at 0 °C. At the end of each experiment the reactor was rapidly cooled at room temperature and slowly degassed. Finally, the liquid reaction mixture was analyzed by Gas Chromatograph coupled with a Flame-Ionization Detector (GC-FID) DANI GC1000, equipped with a HP PONA column (50 m x 0.2 mm x 0.5 µm) in order to determine EtOH conversion and product yields. The reaction products in the liquid phase were also identified by Gas Chromatography-Mass Spectrometry (GC-MS), using a 6890N GC system gas chromatograph coupled with a 5975 mass selective detector single quadrupole mass spectrometer (Agilent Technologies).

The C-balance was always in the range 96-99 %, accounting for a loss of liquid during transfer after reaction, while the absence of ethylene in the gas phase was always ascertained by GC analysis.

The product molar yields Y (mol %), EtOH conversion Conv. (mol %), and selectivity Sel. (mol %) were calculated as:

Y (mol %): (Moles of carbon in the target product / Moles of carbon in fed EtOH) x 100

Conv. (mol %): Moles of reacted EtOH / Moles of fed EtOH) x 100

Sel. (mol %): (Moles of carbon in the target product / Moles of carbon in reacted EtOH) x 100

Space time yield (STY) of product was calculated as STY = g product $kgcat^{-1}$ h^{-1}.

Leaching tests were carried out adopting the following procedure: at the end of the Guerbet reaction the solid catalyst was filtered off under inert atmosphere and the recovered liquid mixture was allowed to proceed for further 6 h.

Results and Discussion

3.1 Synthesis and characterization of the catalysts

The catalyst precursors showed the typical diffraction pattern of pristine HT-type compounds (Figure 1a) (Cavani et al., 1991), in agreement with the incorporation of the Jahn-Teller distorted Cu^{2+} into the brucite-type sheets, favored by the presence of Mg^{2+} (Kannan et al., 2005).

Figure 1, near here

The HT precursors were macroporous or non porous materials that agglomerated forming interparticle slit shaped pores, as revealed by their type IIb N_2 adsorption/desorption isotherms (Rouquerol et al., 2014). The specific surface area values around 70-78 m^2/g were not largely modified with the Cu loading, as evidenced in Table 1.

Table 1, near here

HRTEM images revealed that the samples were constituted by amorphous lamellar nanoparticles (60-70 nm) with rounded edges (Figure S1). EDS analysis confirmed that the composition of the precipitated solids was similar to the theoretical one.

The topotactic decomposition of the lamellar structure took place during calcination at 500 ºC for 7 h. A poorly crystallized MgO-type phase was developed (Figure 1b) wherein Cu^{2+} and Al^{3+} were included forming a mixed oxide (Kannan et al., 2005). The reflections were slightly more intense and narrow as the copper loading decreased. The presence of small CuO clusters in the high loading catalyst was not detectable by XRD, although their presence could not be discarded (Bravo-Suárez et al., 2012). Specific surface area values of calcined samples were around 132-143 m^2/g.

The incorporation of Cu^{2+} species into the oxide structure was supported by H_2-TPR profiles, shown in Figure 2.

Figure 2, near here

H_2 consumption peaks were centred at higher temperatures in comparison to segregated CuO (Han et al., 2016). The onset and maximum of the reduction peaks shifted towards higher temperatures as the copper content decreased, due to better dispersed and stabilised copper species (Chmielarz et al., 2005). The small peak at ca. 630 °C in Cu2.8 and Cu1.0 catalysts could be related to the formation of a copper spinel, e.g. $CuAl_2O_4$ (Alejandre et al., 1999).

The copper content determined by ICPS analysis of the synthesized catalysts Cu7.6, Cu2.8 and Cu1.0 was found to be in very good agreement with the theoretically expected values, resulting 7.58, 2.79 and 1.01 as Cu a.r.% respectively, thus indicating very good incorporation of the metal ions into the hydrotalcite structures.

The basicity of the catalysts was evaluated by CO_2-TPD measurements, reported in Figure 3.

Figure 3, near here

The evolution of CO_2 occurred in the 50-500 °C range, characteristic of HT-derived catalysts containing basic sites of different strength (Di Cosimo et al., 1998). The amount of CO_2 desorbed decreased as the Cu content increased, as highlighted in Table 2.

Table 2, near here

The desorption profiles showed an asymmetric shape that can be deconvoluted into three peaks related to weak (around 105-110 °C), medium (135-145 °C) and strong (234-252 °C) basic sites, attributed to weakly basic Brønsted OH groups, Mg-O Lewis surface pairs and Lewis O^{2-} groups. The three catalysts contained a larger amount of strong basic sites than low and medium sites, which decreased for higher Cu loadings in the catalyst formulation.

3.2 Catalytic conversion of EtOH

The catalytic performances of the three calcined catalysts were compared for the EtOH condensation carried out at 215 °C, adopting similar amounts of MgO basic component and a ratio MgO/EtOH in the range 0.066-0.076 mol/mol (Figure 4).

Figure 4, near here

Figure 4 reveals that this temperature is enough to reach interesting conversion levels for each tested system. At short reaction times (3-6 h) a progressive increase of the substrate conversion was observed moving from Cu7.6 to Cu1.0, i.e. decreasing the concentration of the Cu hydrogenating/dehydrogenating component and increasing the number of basic sites, mainly the strong ones. In fact, Cu1.0 allowed at 215 °C, after 6 h a substrate conversion of 24.7 mol % with a selectivity in BuOH of 53 mol % (Figure 4a). The main by-products resulted higher alcohols, mainly HexOH (selectivity = 21.6 mol %), and 1-octanol (selectivity = 10.2 mol %), while the selectivity in AcOEt was as little as 2.4 mol %. STY of BuOH was 210, while that of the two higher linear alcohols [BuOH + HexOH] was 293. This result is excellent among the up to now reported heterogeneous catalysts when employed under similar and also higher temperatures (Marcu et al., 2013; Sun et al. 2017). Moreover, the co-production of [BuOH + HexOH] is economically more attractive than that of the sole BuOH, because these are both saleable products, and this conclusion

supports the concept of the Guerbet process, as already recently proposed by Nezam et al. (2019). The Cu content has an even more striking effect on the product distribution. In fact, when the Cu-rich Cu7.6 system was employed (Figure 4c) not only a lower EtOH conversion (18.1 mol %) was obtained, with a selectivity in BuOH of 56 mol %, but AcOEt resulted the main by-product (selectivity = 27.4 mol %), HexOH selectivity being only 4.0 mol % after 6 h of reaction. Cu2.8 showed an intermediate behavior, in terms of activity and selectivity (Figure 4b). These results underline the relevant role of Cu content on the catalytic performances, previously reported for this reaction using much less active Cu-Mg-Al mixed oxide catalysts (Marcu et al., 2009). The loading determined the copper reducibility and basicity in the fresh catalysts, as previously commented, and possibly the copper particle size. In addition, in order to exclude Cu leaching from the employed systems, the liquid mixture recovered by filtration after 6 h of reaction at 215 °C in the presence of Cu7.6 was allowed to proceed for further 6 h under the same reaction conditions and no further advancement of the reaction was ascertained, supposing the absence of Cu leaching. This result was additionally confirmed by ICPS analysis of the final liquid mixture recovered after 12 h of reaction which excluded Cu leaching, highlighting as the employed catalysts work in heterogeneous phase.

The characterization of the spent samples revealed, however, structural and morphological changes in the catalysts during reaction conditions altering the catalyst properties.

The structure and therefore the basicity of the samples were modified under the reaction conditions, as evidenced in Figure 5a.

Figure 5, near here

The HT layered structure was reconstructed (Figure 5a) due to the memory effect of the mixed oxides in presence of co-produced water, i.e. 1 mol H_2O per mol BuOH (Sato et al., 1988). Anions, such as ethoxy and butoxy could be intercalated in the interlayer region adopting different configurations (Gardner et al., 2001; Wang et al., 2014), in agreement with the shift of the basal reflections towards lower diffraction angles than in the original HT compound. As a result of the structural transformation, medium Mg-O and strong O^{2-} Lewis basic sites in the calcined catalysts were removed in the hydrated sample (Di Cosimo et al., 1998; Marcu et al., 2009; Prinetto et al., 2000). Thus, though according to CO_2-TPD, the Cu1.0 catalyst showed the largest number of basic sites, prone to promote the condensation step, it was not straightforward to make a comparison between original basicity in the original catalyst and the real one during catalytic tests. On the other hand, the intercalated alkoxy or OH^- anions were Brønsted basic sites. The former have been reported to catalyse the Guerbet condensation both in heterogeneous (Carlini et al., 2004) and homogeneous processes (Chakraborty et al., 2015). Besides, Mg/Al HT compounds intercalated

with tert-butoxide were a strong heterogeneous base in transterification reactions (Fu et al., 2017). On the other hand, OH^- intercalated Mg/Al HT compounds are well-known catalysts in aldol condensation. Indeed, partially decomposed hydrotalcite-type compounds were used for Guerbet reaction (Tsuchida et al., 2001). However, for intercalated samples the accessibility of the reagents to the basic active sites should be considered, since only the anions near the edges of the HT platelet particles may be available (Winter et al., 2006).

The activity seemed not to be directly related to the Cu particle size, but mainly to Cu content, which also controlled oxidation state and chemical environment. In both spent Cu7.6 and Cu1.0, spherical and ill-shaped Cu particles deposited over nanoparticles and large HT platelets were ascertained (Figure 6a, 6b, 6f, 6g). The EDS spectra in the nanoparticles and HT platelets showed a decrease of Cu content (close to zero in 2 and 4) due to the reduction of Cu^{2+}. The large and broad Cu size distribution (Figure 6e, 6i) could be due to the coalescence of the particles during reaction conditions, visible in Figure 6h. Moreover, some trigonal and hexagonal particles probably related to Cu_2O were identified (Figure 6c, 6d); indeed, Cu/O atomic ratio in the particle in Fig. 6c was 1.9.

Figure 6, near here

Copper was partially reduced to Cu^0, as revealed by XRD (Figure 5a) and XPS measurements summarized in Table 3 and Figures S2 and S3. In the spectra of Cu7.6, the main Cu2$p_{3/2}$ signal was composed of two contributions at 932.9 and 934.8 eV due to Cu^0 and Cu^{2+} probably on the mixed oxide (Crivello et al., 2005), which shifted towards lower values, 931.6 and 933.6 eV, in Cu1.0 spectra due to metallic copper and the spinel $CuAl_2O_4$, respectively, together with Cu^{2+} in the mixed oxide. The ratio of the areas of the satellite region and the main signal (I_{sat}/I_{mp}) and the Cu^0/Cu^{2+} ratio, which modified the hydrogenating/dehydrogenating activity, resulted metal loading dependent. The amount of Cu^0 species increased with the copper loading, in agreement with H_2-TPR results, wherein more difficulty reducible species were identified in Cu1.0 rather than in Cu7.6. Thus, the Cu7.6 catalyst had a higher dehydrogenating activity favouring the formation of intermediate acetaldehyde, which then gives AcOEt by dehydrogenative route involving the hemiacetal (Inui et al., 2004).

A very interesting result was reached when the condensation was carried out using the same catalysts after a pre-reduction step at 180 °C in MeOH under 5 MPa of H_2, as shown in Figure 7.

Figure 7, near here

A positive effect of the prereduction was ascertained for Cu1.0 and Cu2.8. When pre-reduced Cu1.0 was tested, after 6 h at 215 °C EtOH conversion reached 29.8 mol %, with a selectivity in BuOH of 57.4 mol % (corresponding to a STY of BuOH of 270). On the other hand, in the case of Cu7.6, the

pre-reduction caused a low decrease of the activity and a significant drop of the selectivity in BuOH (from 56.6 to 37.7 mol % after 6 h, with a corresponding increase of that in AcOEt up to 53.4 mol %). The pre-reduction modified the copper particle size (Figure 8) rather than the oxidation state (Table 3 and Figures S2 and S3) in the spent catalysts and consequently their activity in dehydrogenation/hydrogenation steps.

Figure 8, near here

The pretreatment reduced the sintering, an effect more remarkable at low Cu-loading, i.e. the copper particle sizes in Cu7.6 were in the 10-60 nm range (Figure 8a, 8d), while Cu1.0 contained well dispersed 1 to 10 nm particles (Figure 8e, 8g), together with particles up to 135 nm (Figure 8f, 8h). The decrease in the particle size in both catalysts could enhance the activities previously commented, namely the formation of the esters for the high Cu-loaded catalyst and the BuOH production for the low Cu-loaded one. The spent Cu7.6 catalyst, which produced lower BuOH, generated less water and was less rehydrated than Cu2.8 and Cu1.0 (Figure 5b); this may also contribute to the preservation of some properties of the catalyst after reduction (Figures S4 and S5), although the sintering by coalescence also happened (Figure 8b, 8c).

The best catalytic system Cu1.0 was also tested at 230 °C and the results are reported in Table 4.

Table 4, near here

The temperature increase caused an increase of the activity, mainly at short reaction time: after 3 h at 230 °C, STY of BuOH reached 372, a remarkable result up to now never reported to date in the literature for this reaction performed under similar conditions.

On the basis of the achieved results, e.g. taking into account the best catalytic performances for the BuOH production, the Cu1.0 catalyst was identified as the best one (Figure 4a and Table 4) and it was further considered for a preliminary recyclability study. The recovered catalyst was tested i) after EtOH washing and calcination at 500 °C for 7 h, and ii) after EtOH washing. The recycle data were compared with the performances of the first cycle (Figure 9):

Figure 9, near here

The obtained results appeared remarkable: calcination allowed to almost completely restore the catalytic performances (compare Fig 9a with 9b), due to the regeneration of the starting catalyst basicity. On the other hand, when a simple EtOH washing was adopted, lower yields were reached, the ascertained activity being ascribed to the intercalated alkoxy or OH^- basic sites in the reconstructed HT-type structure.

In order to confirm the importance of a low Cu content to achieve high yields in higher alcohols and reduce the amount of formed ester, the effect of the progressive reduction of the copper-rich Cu7.6

amount was studied, compensating for the low amount of Mg/Al mixed oxide species by adding those derived from a commercial HT compound (MG Puralox). The results reported in Figure 10 perfectly confirm that the lowering of the introduced Cu amount, if the depletion of Mg/Al component is counterbalanced, leads to complete turn of the catalytic behavior.

Figure 10, near here

In fact, moving from the pure Cu7.6 catalyst (Figure 9a) to decreasing Cu7.6 amounts (Figure 9b, 9c), a progressive increase of the conversion and, above all, a marked enhancement of the selectivity in higher alcohols was observed at expense of the AcOEt formation. When 1 mmol of Cu was employed (run c in Figure 9) the results were quite similar to those obtained in run a) of Figure 4 where the catalyst Cu1.0 with the lowest loading was adopted, i.e. using the same amount of Cu. In fact, in this case, after 6 h, the EtOH conversion of 22 mol % was reached with selectivity in BuOH of 58.1 mol %. Also in this case, the main by-product turned to HexOH (selectivity = 18.2 mol %), while the selectivity in AcOEt dropped to 4.3 mol %. After 6 h, the STY considering the introduced Cu7.6 system resulted 705, the highest value up to now reported using Cu-based systems.

On the other hand, when only the Cu-free Mg/Al system was employed (Figure 9d) the activity was very low (EtOH conversion = 3.6 mol % after 6 h) but the selectivity to BuOH reached 67 mol %. These results underline the importance of the copper component, although in low concentration, in the mixed oxide and confirm the best performances ascertained for the Cu1.0 system.

For all the catalysts tested at 215 °C a decrease of the catalytic performances was observed as the reaction continued (Figure 4), due to water accumulated in the batch reactor which caused the reconstruction of the HT-type structure with the intercalation in the interlayer region of both OH^- and large anions, probably alkoxy species (Figure 5). The reconstruction modified the Cu particle size and the type and accessibility of the basic sites.

Therefore, the effect of water removal was studied, by addition of anhydrous $MgSO_4$, as reported in Figure 11.

Figure 11, near here

As previously observed by Marcu et al. (2009), the addition of the drying agent enhanced the catalytic activity: EtOH conversion after 12 h moved from 28.2 to 34.7 mol % and also the selectivity in BuOH was slightly increased. These positive effects of the water removal could be related to the preservation of Lewis stronger basic sites O^{2-} rather than their transformation into weaker Brønsted OH^- ones. In the case of higher linear C_8, C_{10} and C_{18} alcohols, Guerbet condensation in the presence of Ni/Cu hydrotalcite derived mixed oxides, a high catalytic stability

is ascertained when water is continuously removed using a with a Dean–Stark azeotrope trap (Hernandez et al., 2016).

Conclusions

Targeting the EtOH conversion to BuOH or to Guerbet alcohols [BuOH + HexOH] may face economic challenges in the immediate future, and the Guerbet approach shifts the focus from the not-sustainable fossil-based "oxo" process to an extremely attractive conversion of renewable resources, competitive respect to the bio-chemical path ("ABE" fermentation process). However, Guerbet reaction still needs optimization to reach good yields to target products at subcritical temperature, at the same time attaining a high carbon yield. For this purpose, new green catalysts must be properly designed and characterized, thus establishing structure-performance trends, and further improving the economy/sustainability of this reaction. The tailoring in the Cu-content in hydrotalcite-derived Cu/Mg/Al mixed oxides allowed us to obtain good performances in the Guerbet condensation of EtOH to BuOH, carried out in the liquid phase at moderate temperatures. The synthesis of Cu-HT catalysts is cheap, easy and reproducible, based on available, safe and inexpensive metals, thus representing excellent alternatives to the rare and expensive noble-metal catalysts. In addition, these catalysts have showed a good recyclability, in term of catalytic performances to [BuOH + HexOH]. A very notable advantage of the adopted systems is the possibility of modulation of their acid-base properties addressing the process towards Guerbet alcohols. In fact, the possibility to selectively co-produce the two linear alcohols [BuOH + HexOH] is economically more advantageous than to produce only BuOH, being both valuable products. In this context, a low Cu-content was required to decrease the ester formation and favour the aldol condensation to BuOH and higher alcohols. The differences in the activity and selectivity were related to the metallic/acid/basic sites in the fresh catalysts, a decrease in the Cu content increasing the basic sites and decreasing Cu reducibility. Besides, the original HT structure was partially reconstructed under the adopted reaction conditions due to the co-produced water, Cu^{2+} partially reduced and copper particles sintered, therefore modifying the type and accessibility of basic and metallic sites. The catalyst Cu1.0 with the lowest Cu loading contained a lower Cu^{0}/Cu^{2+} ratio after catalytic tests than a high loaded one, thus providing less hydrogenation sites and decreasing the ester formation. A pre-reduction treatment delayed the sintering and enhanced the activities in alcohol and ester formation for low and high loaded catalysts, respectively. These tunable performances can be further enhanced by removing the co-produced water which caused the

reconstruction of the HT structure, by adding a drying agent, while the study of this reaction in flow-reactor is now in progress.

References

Alejandre, A., Medina, F., Salagre, P., Correig, X., Sueiras, J.E., 1999. Preparation and study of Cu-Al mixed oxides via hydrotalcite-like precursors. Chem. Mater. 11, 939–948. https://doi.org/10.1021/cm980500f.

Bravo-Suárez, J.J., Subramaniam, B., Chaudhari, R.V., 2012. Ultraviolet-visible spectroscopy and temperature-programmed techniques as tools for structural characterization of Cu in $CuMgAlO_x$ mixed metal oxides. J. Phys. Chem. C 116, 18207–18221. https://doi.org/10.1021/jp303631v.

Carlini, C., Flego, C., Marchionna, M., Noviello, M., Raspolli Galletti, A.M., Sbrana, G., Basile, F., Vaccari, A., 2004. Guerbet condensation of methanol with *n*-propanol to isobutyl alcohol over heterogeneous copper chromite/Mg-Al mixed oxides catalysts. J. Mol. Catal. A 220, 215–220. https://doi.org/10.1016/j.molcata.2004.05.034.

Carlini, C., Marchionna, M., Noviello, M., Raspolli Galletti, A.M., Sbrana, G., Basile, F., Vaccari, A., 2005. Guerbet condensation of methanol with *n*-propanol to isobutyl alcohol over heterogeneous bifunctional catalysts based on Mg-Al mixed oxides partially substituted by different metal components. J. Mol. Catal. A 232, 13–20. https://doi.org/10.1016/j.molcata.2004.12.037.

Carvalho, D.L., de Avillez, R.R., Rodrigues, M.T., Borges, L.E.P., Appel, L.G., 2012. Mg and Al mixed oxides and the synthesis of *n*-butanol from ethanol. Appl. Catal. A: Gen. 415–416, 96–100. https://doi.org/10.1016/j.apcata.2011.12.009.

Cavani, F., Trifiró, F., Vaccari, A., 1991. Hydrotalcite-type anionic clays: Preparation, properties and applications. Catal. Today 11, 173–301. https://doi.org/10.1016/0920-5861(91)80068-K.

Chakraborty, S., Piszel, P.E., Hayes, C.E., Baker, R.T., Jones, W.D., 2015. Highly selective formation of *n*-butanol from ethanol through the Guerbet process: A tandem catalytic approach. J. Am. Chem. Soc. 137, 14264–14267. https://doi.org/10.1021/jacs.5b10257.

Chieregato, A., Velasquez Ochoa, J., Bandinelli, C., Fornasari, G., Cavani, F., Mella, M., 2015. On the chemistry of ethanol on basic oxides: Revising mechanisms and intermediates in the Lebedev and Guerbet reactions. ChemSusChem 8, 377–388. https://doi.org/10.1002/cssc.201402632.

Chmielarz, L., Kuśtrowski, P., Rafalska-Łasocha, A., Dziembaj, R., 2005. Selective oxidation of ammonia to nitrogen on transition metal containing mixed metal oxides. Appl. Catal. B: Environ. 58, 235–244. https://doi.org/10.1016/j.apcatb.2004.12.009.

Crivello, M., Pérez, C., Herrero, E., Ghione, G., Casuscelli, S., Rodriguez-Castellón, E., 2005. Characterization of Al-Cu and Al-Cu-Mg mixed oxides and their catalytic activity in dehydrogenation of 2-octanol. Catal. Today 107–108, 215–222. https://doi.org/10.1016/j.cattod.2005.07.168.

Di Cosimo, J.I., Apesteguía, C.R., Ginés, M.J.L., Iglesia, E., 2000. Structural requirements and reaction pathways in condensation reactions of alcohols on Mg_yAlO_x catalysts. J. Catal. 190, 261–275. https://doi.org/10.1006/jcat.1999.2734.

Di Cosimo, J.I., Díez, V.K., Xu, M., Iglesia, E., Apesteguía, C.R., 1998. Structure and surface and catalytic properties of Mg-Al basic oxides. J. Catal. 178, 499–510. https://doi.org/10.1006/jcat.1998.2161.

Dowson, G.M.R., Haddow, M.F., Lee, J., Wingad, R.L., Wass, D.F., 2013. Catalytic conversion of ethanol into an advanced biofuel: Unprecedented selectivity for n-butanol. Angew. Chem. Int. Ed. 52, 9005–9008. https://doi.org/10.1002/anie.201303723.

Fu, S., Shao, Z., Wang, Y., Liu, Q., 2017. Manganese-catalyzed upgrading of ethanol into 1-butanol. J. Am. Chem. Soc. 139, 11941–11948. https://doi.org/10.1021/jacs.7b05939.

Gabriëls, D., Hernández, W.Y., Sels, B., Van Der Voort, P., Veberckmoes, A., 2015. Review of catalytic systems and thermodynamics for the Guerbet condensation reaction and challenges for biomass valorization. Catal. Sci. Technol. 5, 3876–3902. https://doi.org/10.1039/C5CY00359H.

Gardner, E., Huntoon, K.M., Pinnavaia, T.J., 2001. Direct synthesis of alkoxide-intercalated derivatives of hydrotalcite-like layered double hydroxides: Precursors for the formation of colloidal layered double hydroxide suspensions and transparent thin films. Adv. Mater. 13, 1263–1266. https://doi.org/10.1002/1521-4095(200108)13:163.0.CO;2-R.

Han, J., Zeng, H.-Y., Xu, S., Chen, C.-R., Liu, X.-J., 2016. Catalytic properties of CuMgAlO catalyst and degradation mechanism in CWPO of methyl orange. Appl. Catal. A: Gen. 527, 72–80. https://doi.org/10.1016/j.apcata.2016.08.015.

Hashim, H., Narayanasamy, M., Yunus, N.A., Shiun, L.J., Muis, Z.A., Ho, W.S., 2017. A cleaner and greener fuel: Biofuel blend formulation and emission assessment. J. Clean. Prod. 146, 208-217. https://doi.org/10.1016/j.jclepro.2016.06.021.

Hernández, W.Y., De Vlieger, K., Van Der Voort, P., Verberckmoes, A., 2016. Ni−Cu hydrotalcite-derived mixed oxides as highly selective and stable catalysts for the synthesis of β-branched bioalcohols by the Guerbet reaction. ChemSusChem, 9, 3196-3205. https://doi.org/10.1002/cssc.201601042.

Hosoglu, F., Faye, J., Mareseanu, K., Tesquet, G., Miquel, P., Capron, M., Gardoll, O., Lamonier, J.-F., Lamonier, C., Dumeignil, F., 2015. High resolution NMR unraveling Cu substitution of Mg in hydrotalcites-ethanol reactivity. Appl. Catal. A: Gen. 504, 533–541. https://doi.org/10.1016/j.apcata.2014.10.005.

Inui, K., Kurabayashi, T., Sato, S., Ichikawa, N., 2004. Effective formation of ethyl acetate from ethanol over Cu-Zn-Zr-Al-O catalyst. J. Mol. Catal. A 216, 147–156. https://doi.org/10.1016/j.molcata.2004.02.017.

Jafari, Y., Karimi, K., Amiri, H., 2017. Efficient bioconversion of whole sweet sorghum plant to acetone, butanol, and ethanol improved by acetone delignification. J. Clean. Prod. 166, 1428-1437. https://doi.org/10.1016/j.jclepro.2017.08.132.

Kannan, S., Dubey, A., Knözinger, H., 2005. Synthesis and characterization of CuMgAl ternary hydrotalcites as catalysts for the hydroxylation of phenol. J. Catal. 231, 381–392. https://doi.org/10.1016/j.jcat.2005.01.032.

León, M., Díaz, E., Ordóñez, S., 2011. Ethanol catalytic condensation over Mg-Al mixed oxides derived from hydrotalcites. Catal. Today 164, 436–442. https://doi.org/10.1016/j.cattod.2010.10.003.

Li, X.N., Peng, S.S., Feng, L.N., Lu, S.Q., Ma, L.J., Yue, M.B., 2018. One-pot synthesis of acidic and basic bifunctional catalysts to promote the conversion of ethanol to 1-butanol. Microporous Mesoporous Mater. 261, 44–50. https://doi.org/10.1016/j.micromeso.2017.11.004.

Machado, C.F.R., Araújo, O.Q.F., Medeiros, J.L., Alves, R.M.B., 2018. Carbon dioxide and ethanol from sugarcane biorefinery as renewable feedstocks to environment-oriented integrated chemical plants. J. Clean. Prod. 172, 1232–1242. https://doi.org/10.1016/j.jclepro.2017.10.234.

Marcu, I.-C., Tanchoux, N., Fajula, F., Tichit, D., 2013. Catalytic conversion of ethanol into butanol over M-Mg-Al mixed oxide catalysts (M = Pd, Ag, Mn, Fe, Cu, Sm, Yb) obtained from LDH precursors. Catal. Lett. 143, 23–30. https://doi.org/10.1007/s10562-012-0935-9.

Marcu, I.-C., Tichit, D., Fajula, F., Tanchoux, N., 2009. Catalytic valorization of bioethanol over Cu-Mg-Al mixed oxide catalysts. Catal. Today 147, 231–238. https://doi.org/10.1016/j.cattod.2009.04.004.

Nezam, I., Peereboom, L., Miller, D.J., 2019. Continuous condensed-phase ethanol conversion to higher alcohols: Experimental results and techno-economic analysis, J. Clean. Prod. In press. https://doi.org/10.1016/j.jclepro.2018.10.276.

Pang, J., Zheng, M., He, L., Li, L., Pan, X., Wang, A., Wang, X., Zhang, T., 2016. Upgrading ethanol to *n*-butanol over highly dispersed Ni-MgAlO catalysts. J. Catal. 344, 184–193. https://doi.org/10.1016/j.jcat.2016.08.024.

Pereira, L.G., Chagas, M.F., Dias, M.O.S., Cavalett, O., Bonomi, A., 2015. Life cycle assessment of butanol production in sugarcane biorefineries in Brazil. J. Clean. Prod. 96, 557-568. https://doi.org/10.1016/j.jclepro.2014.01.059.

Prinetto, F., Ghiotti, G., Durand, R., Tichit, D., 2000. Investigation of acid-base properties of catalysts obtained from layered double hydroxides. J. Phys. Chem. B 104, 11117–11126. https://doi.org/10.1021/jp002715u.

Riittonen, T., Salmi, T., Mikkola, J.-P., Wärnå, J., 2014. Direct synthesis of 1-butanol from ethanol in a plug flow reactor: Reactor and reaction kinetics modeling. Top. Catal. 57, 1425–1429. https://doi.org/10.1007/s11244-014-0314-4.

Rouquerol, F., Rouquerol, J., Sing, K.S.W., Llewellyn, P., Maurin, G., 2014. Adsorption by powders and porous solids. Principles, methodology and applications, second ed. Academic Press, Oxford.

Sato, T., Fujita, H., Endo, T., Shimada, M., Tsunashima, A., 1988. Synthesis of hydrotalcite-like compounds and their physico-chemical properties. React. Solids 5, 219–228. https://doi.org/10.1016/0168-7336(88)80089-5.

Sreekumar, S., Balakrishnan, M., Goulas, K., Gunbas, G., Gokhale, A.A., Louie, L., Grippo, A., Scown, C.D., Bell, A.T., Toste, F.D., 2015. Upgrading lignocellulosic products to drop-in biofuels via dehydrogenative cross-coupling and hydrodeoxygenation sequence, ChemSusChem 8, 2609-2614. https://doi.org/10.1002/cssc.201500754.

Sun, Z., Vasconcelos, A.C., Bottari, G., Stuart, M.C.A., Bonura, G., Cannilla, C., Frusteri, F., Barta, K., 2017. Efficient catalytic conversion of ethanol to 1-butanol via the Guerbet reaction over copper- and nickel-doped porous. ACS Sustainable Chem. Eng. 5, 1738–1746. https://doi.org/10.1021/acssuschemeng.6b02494.

Tsuchida, T., Atsumi, K., Sakuma, S., Inui, T., 2001. Synthesis method of chemical industrial raw material and high-octane fuel, and high-octane fuel composition. Patent US 6,323,383 B1.

Wang, H., Duan, W., Wu, Y., Tang, Y., Li, L., 2014. Synthesis of magnesium-aluminum layered double hydroxide intercalated with ethylene glycol by the aid of alkoxides. Inorg. Chim. Acta 418, 163–170. https://doi.org/10.1016/j.ica.2014.04.031.

Winter, F., Xia, X., Hereijgers, B.P.C., Bitter, J.H., Van Dillen, A.J., Muhler, M., De Jong, K.P., 2006. On the nature and accessibility of the Brønsted-base sites in activated hydrotalcite catalysts. J. Phys. Chem. B 110, 9211–9218. https://doi.org/10.1021/jp0570871.

Wu, X., Fang, G., Tong, Y., Jiang, D., Liang, Z., Leng, W., Liu, L., Tu, P., Wang, H., Ni, J., Li, X. , 2018. Catalytic Upgrading of Ethanol to n-Butanol: Progress in Catalyst Development ChemSusChem, 11 (1), 71-85. https://doi.org/10.1002/cssc.201701590.

Zhang, Q., Dong, J., Liu, Y., Wang, Y., Cao, Y., 2016. Towards a green bulk-scale biobutanol from bioethanol upgrading. J. Energy Chem. 25, 907–910. https://doi.org/10.1016/j.jechem.2016.08.010.

Captions for Figures and Scheme

Figure 1: a) Diffraction patterns of the catalyst precursors Cu7.6 HT, Cu2.8 HT and Cu1.0 HT; b) Diffraction patterns of the catalysts after calcination at 500 ºC for 7 h.

Figure 2: H_2-TPR profiles for the catalysts Cu7.6, Cu2.8 and Cu1.0.

Figure 3: CO_2-TPD profiles and its deconvolution indicating low (red), medium (green) and strong (blue) basic sites for the catalysts Cu7.6, Cu2.8 and Cu1.0.

Figure 4: Influence of Cu loading on the catalytic performances of the different catalysts at temperature 215 °C, EtOH 893 mmol: a) Cu1.0 catalyst, Cu: 1 mmol (MgO 67.9 mmol); b) Cu2.8 catalyst, Cu: 2.68 mmol (MgO 65.9 mmol); c) Cu7.6 catalyst, Cu: 7.1 mmol, (MgO 59.0 mmol). Other products: 2-ethyl-1-hexanol, 1,1-diethoxy-ethane, ethyl butyrate, 2-ethyl-1-butanol, 1-octanol.

Figure 5: a) Diffraction patterns of the spent catalysts Cu7.6, Cu2.8 and Cu1.0 and diffraction pattern of the catalyst precursor Cu1.0 HT; b) Diffraction patterns of the spent pre-reduced catalysts Cu7.6, Cu2.8 and Cu1.0, together with the diffraction pattern of the catalyst precursor Cu1.0 HT.

Figure 6: HRTEM characterization of Cu7.6 and Cu1.0 spent catalysts: HAADF/STEM images (a: Cu7.6; f: Cu1.0), HRTEM images (b, c, d: Cu7.6; g, h: Cu1.0) and particle size distributions (e: Cu7.6; i: Cu1.0).

Figure 7: Influence of the pre-reduction step on the catalytic performances of the different catalytic systems in EtOH condensation at 215 °C, EtOH 893 mmol: a) Cu1.0 catalyst, Cu: 1 mmol (MgO: 68.3 mmol); b) Cu2.8 catalyst, Cu: 2.7 mmol (MgO: 63.4 mmol); c) Cu7.6 catalyst, Cu: 7.1 mmol (MgO: 59.0 mmol). Other products: 2-ethyl-1-hexanol, 1,1-diethoxy-ethane, ethyl butyrate, 2-ethyl-1-butanol, 1-octanol.

Figure 8: HRTEM characterization of Cu7.6 and Cu1.0 pre-reduced spent catalysts: HRTEM images (a, b, c: Cu7.6; f: Cu1.0), HAADF/STEM image (e: Cu1.0), and particle size distributions (d: Cu7.6; g, h: Cu1.0). The table summarizes the atomic ratios obtained from STEM/EDS in selected regions indicated in the images with numbers; the balance to 100% is C from the grid.

Figure 9: Recycling tests of the spent Cu1.0 catalyst - Effect of the reactivation treatment on the catalytic performances. Reaction conditions: EtOH: 893 mmol, Cu: 1 mmol (MgO 67.9 mmol), temperature: 215 °C. a) Direct cycle from Figure 4 a; b) Thermal reactivation by calcination at 500 °C; c) Reactivation by EtOH washing.

Figure 10: Influence of the addition of commercial MG Puralox on the catalytic performances of Cu7.6 catalyst at 215 °C, EtOH 893 mmol: a) Cu7.6 catalyst, Cu: 7.1 mmol (MgO 59.0 mmol), MG Puralox: absent; b) Cu7.6 catalyst, Cu: 3.8 mmol (MgO 31.6 mmol) MG Puralox: 34.2 mmol

of MgO; c) Cu7.6 catalyst, Cu: 1 mmol (MgO 8.3 mmol) MG Puralox: 63.0 mmol of MgO; d) Cu7.6: absent; MG Puralox: 73.1 mmol of MgO. Other products: 2-ethyl-1-hexanol, 1,1-diethoxy-ethane, ethyl butyrate, 2-ethyl-1-butanol, 1-octanol.

Figure 11: Influence of the presence of $MgSO_4$ on the catalytic performances of Cu7.6 at 215 °C, EtOH 893 mmol: a) Cu7.6 catalyst, Cu: 1 mmol, MgO 8.3 mmol, MG Puralox: 63.0 mmol of MgO; b) Cu7.6 catalyst, Cu: 1 mmol; MgO 8.3 mmol, MG Puralox: 63.0 mmol of MgO; $MgSO_4$: 3 g. Other products: 2-ethyl-1-hexanol, 1,1-diethoxy-ethane, ethyl butyrate, 2-ethyl-1-butanol, 1-octanol.

Scheme 1: Reaction network for Guerbet reaction.

Table 1. Specific surface area (SSA) values of the HT precursors, fresh and spent catalysts.

Sample	SSA (m^2/g)			
	HT	**c500[a]**	**Spent**	**Spent pre-reduced**
Cu7.6	71	133	167	180
Cu2.8	75	132	157	175
Cu1.0	78	143	157	170

[a] samples after calcinations at 500°C for 7 h

Table 2. Basicity distribution of the catalysts from CO_2-TPD measurements.

Sample	μmol CO_2 / g_{cat}	Low	Medium	Strong
Cu7.6	215	10 %	15 %	75 %
Cu2.8	276	12 %	16 %	72 %
Cu1.0	358	7 %	11 %	82 %

Table 3. Binding energies of the Cu2p$_{3/2}$ peaks, values of I_{sat}/I_{mp} and Cu^0/Cu^{2+} ratio for the Cu7.6 and Cu1.0 pre-reduced and not pre-reduced spent catalysts.

Sample	Prereduction	Peak	Position (eV)	I_{sat}/I_{mp}	Cu^0/Cu^{2+}
Cu7.6	No	Cu 2$p_{3/2}$	932.9 934.8	0.11	2.23
Cu7.6	Yes		932.8 934.8	0.20	1.78
Cu1.0	No		931.6 933.6	0.35	0.39
Cu1.0	Yes		931.9 933.5	0.40	0.32

Table 4. Effect of the temperature on EtOH condensation in the presence of Cu1.0 catalyst. Reaction conditions: EtOH 893 mmol, Cu: 1 mmol (MgO 67.9 mmol).

Temperature (°C)	Time (h)	Conv. (mol %)	Selectivity (mol %)			
			BuOH	AcOEt	HexOH	Others
215	3	15.8	56.0	3.1	20.0	20.9
	6	24.7	53.0	2.4	21.6	22.7
	12	27.8	52.8	2.5	21.7	23.0
230	3	21.0	55.8	3.5	26.2	14.5
	6	26.1	57.5	3.4	18.9	20.2
	12	32.4	52.1	3.3	19.9	24.3

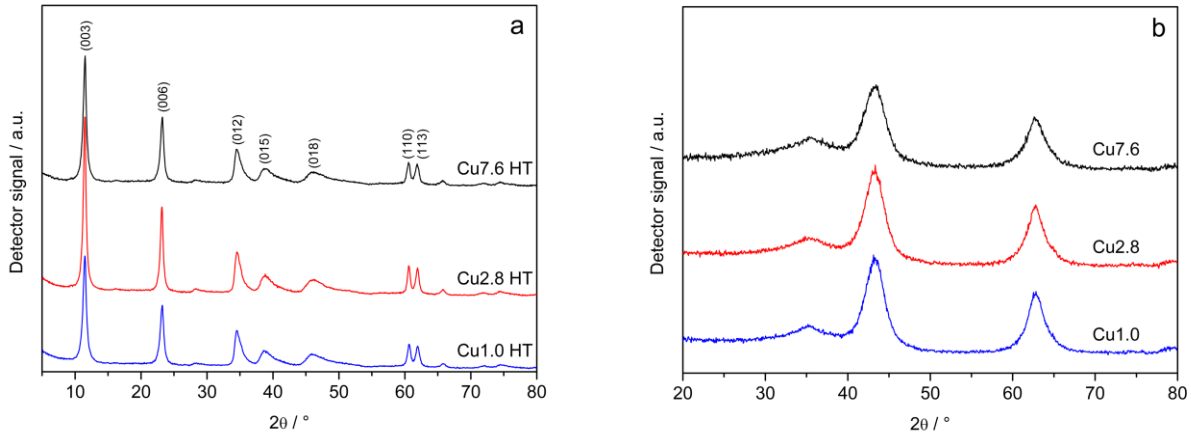
a
(003)
(006)
(012)
(015)
(018)
(110)
(113)
Cu7.6 HT
Cu2.8 HT
Cu1.0 HT
Detector signal / a.u.
10
20
30
40
50
60
70
80
2θ / °
b
Cu7.6
Cu2.8
Cu1.0
Detector signal / a.u.
20
30
40
50
60
70
80
2θ / °

Figure 1

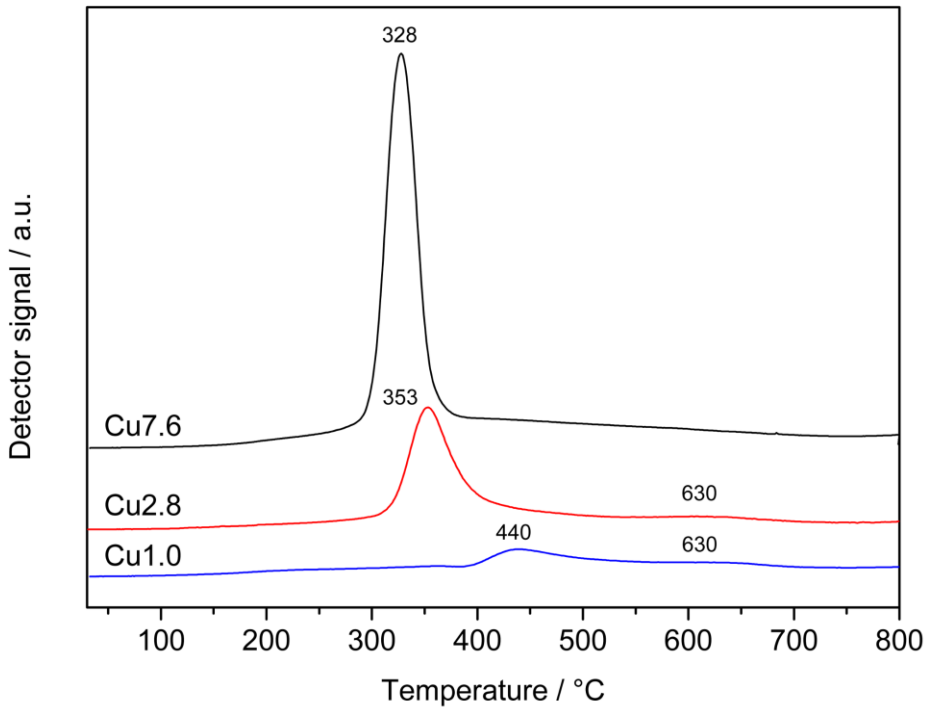
328
353
630
440
630
Cu7.6
Cu2.8
Cu1.0
Detector signal / a.u.
100
200
300
400
500
600
700
800
Temperature / °C

Figure 2

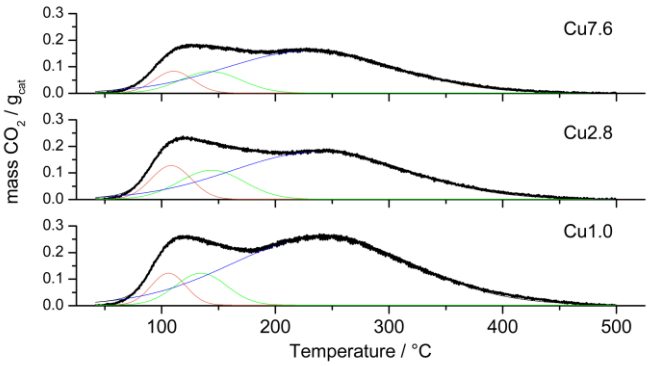
Cu7.6
Cu2.8
Cu1.0
mass CO_2 / g_{cat}
0.0
0.1
0.2
0.3
100
200
300
400
500
Temperature / °C

Figure 3

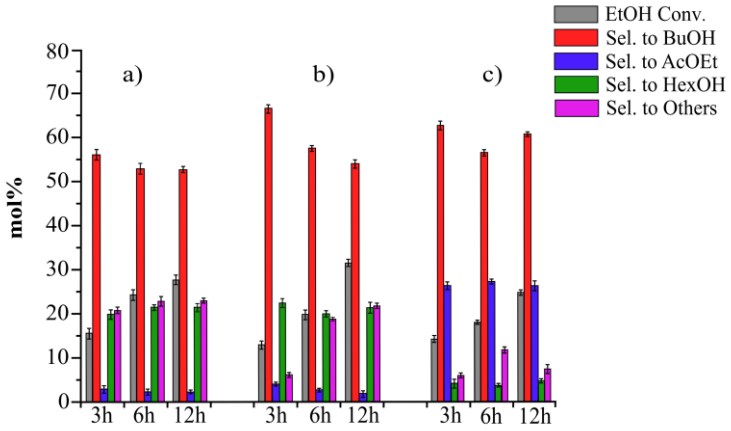
EtOH Conv.
Sel. to BuOH
Sel. to AcOEt
Sel. to HexOH
Sel. to Others
a)
b)
c)
mol%
0
10
20
30
40
50
60
70
80
3h
6h
12h
3h
6h
12h
3h
6h
12h

Figure 4

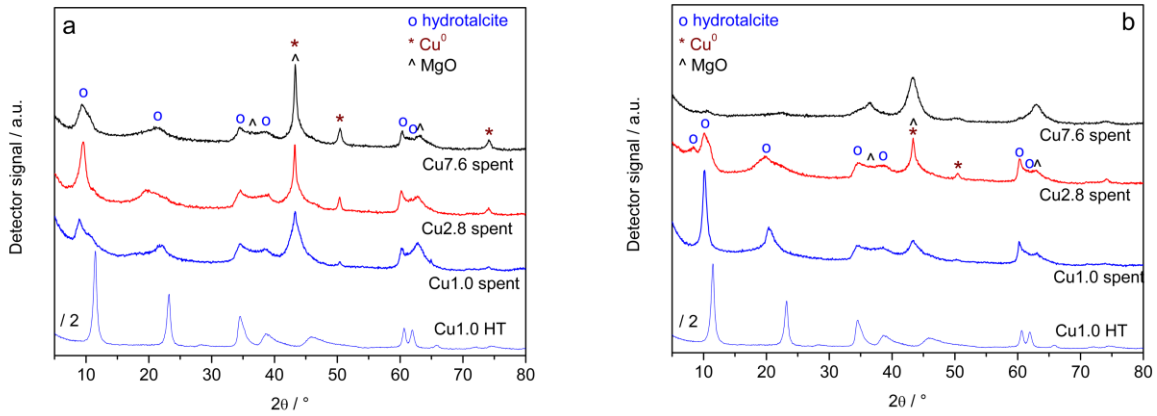
a
o hydrotalcite
* Cu0
^ MgO
Cu7.6 spent
Cu2.8 spent
Cu1.0 spent
/ 2
Cu1.0 HT
Detector signal / a.u.
2θ / °
b
o hydrotalcite
* Cu0
^ MgO
Cu7.6 spent
Cu2.8 spent
Cu1.0 spent
/ 2
Cu1.0 HT
Detector signal / a.u.
2θ / °

Figure 5

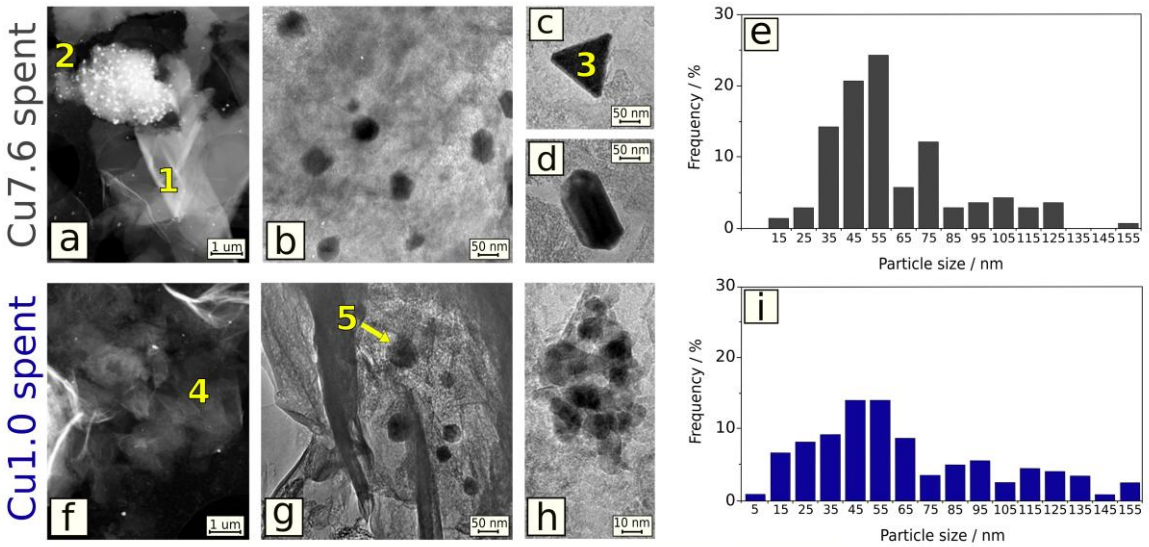

Element (a.r.%)	1	2	3	4	5
Mg	22.7	40.5	0	38.1	32.0
Al	16.4	9.8	0	12.7	7.7
Cu	1.3	0	65.4	0.3	16.1
O	54.2	47.1	34.6	48.9	44.2

Figure 6

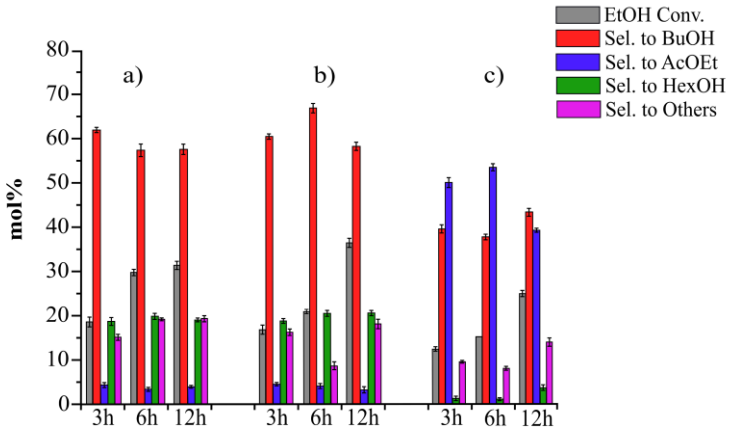
EtOH Conv.
Sel. to BuOH
Sel. to AcOEt
Sel. to HexOH
Sel. to Others
mol%
a)
b)
c)
0
10
20
30
40
50
60
70
80
3h
6h
12h
3h
6h
12h
3h
6h
12h

Figure 7

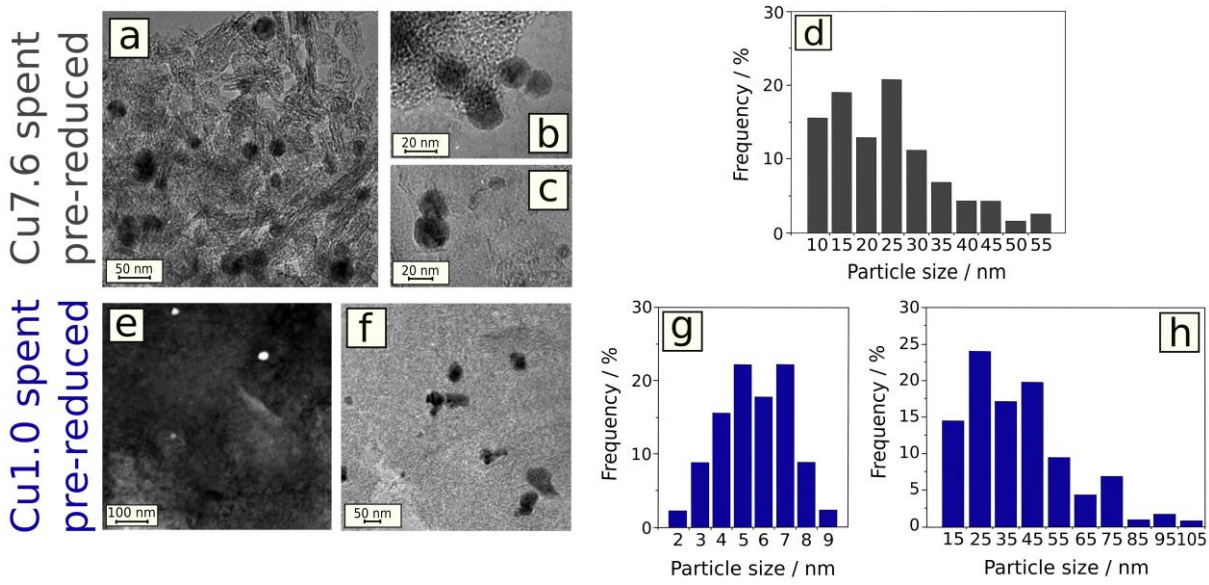
Cu7.6 spent pre-reduced
Cu1.0 spent pre-reduced
a
b
c
d
e
f
g
h
50 nm
20 nm
20 nm
100 nm
50 nm
Frequency / %
Particle size / nm
Frequency / %
Particle size / nm
Frequency / %
Particle size / nm

Figure 8

Figure 9

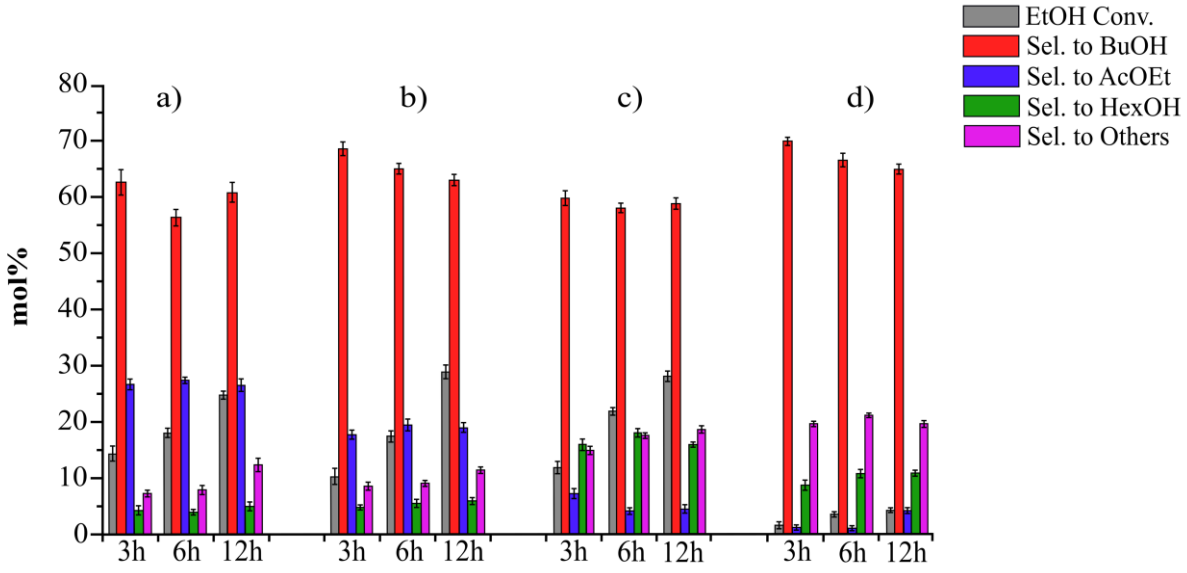
EtOH Conv.
Sel. to BuOH
Sel. to AcOEt
Sel. to HexOH
Sel. to Others
mol%
a)
b)
c)
d)
0
10
20
30
40
50
60
70
80
3h
6h
12h

Figure 10

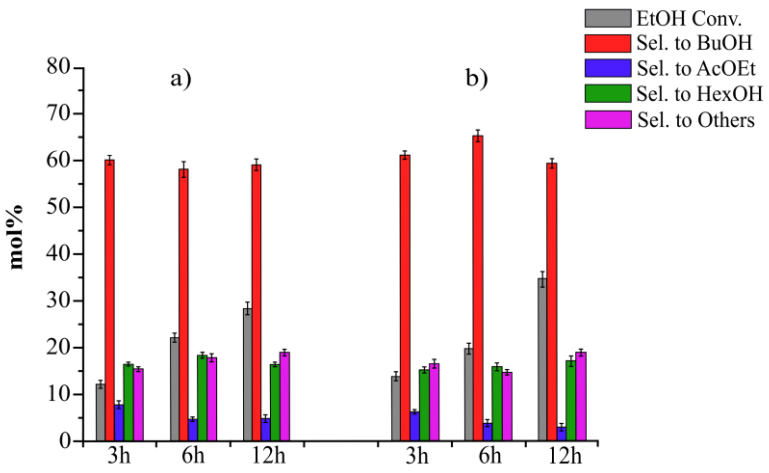
EtOH Conv.
Sel. to BuOH
Sel. to AcOEt
Sel. to HexOH
Sel. to Others
a)
b)
mol%
0
10
20
30
40
50
60
70
80
3h
6h
12h
3h
6h
12h

Figure 11

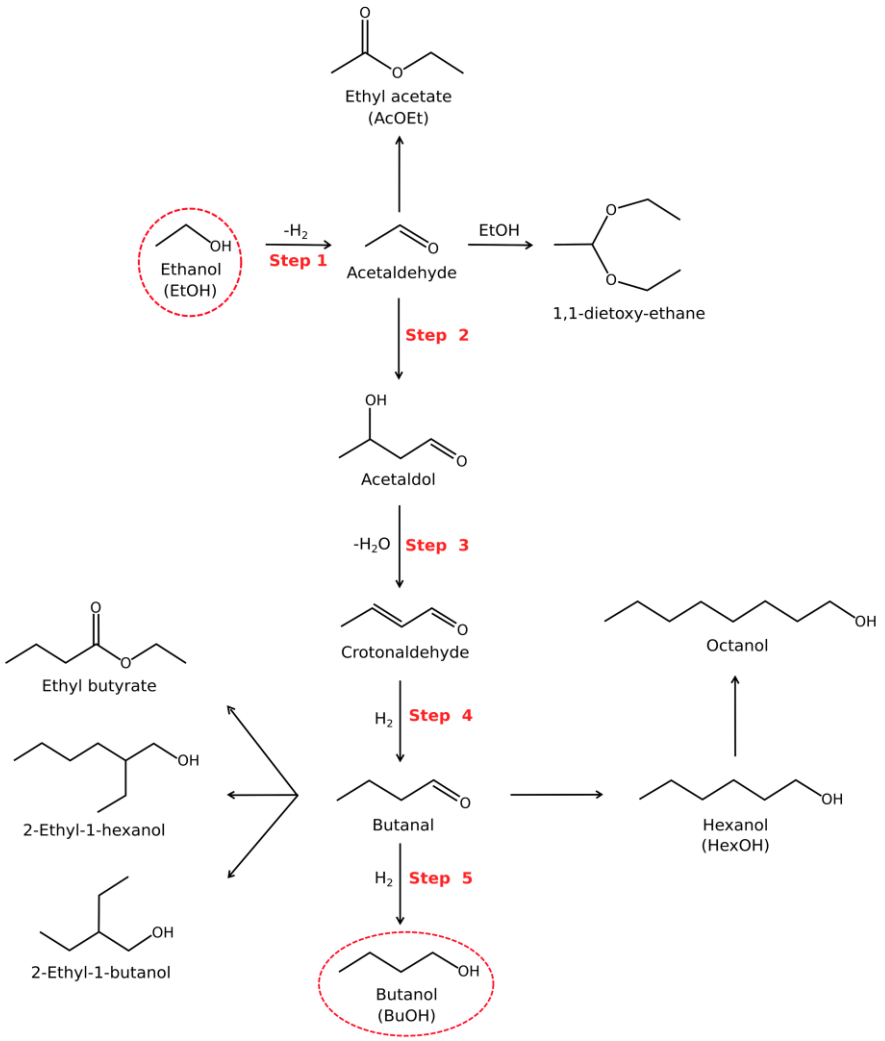
Ethyl acetate
(AcOEt)
Ethanol
(EtOH)
-H2
Step 1
Acetaldehyde
EtOH
1,1-dietoxy-ethane
Step 2
Acetaldol
-H2O
Step 3
Crotonaldehyde
Ethyl butyrate
Octanol
H2
Step 4
2-Ethyl-1-hexanol
Butanal
Hexanol
(HexOH)
H2
Step 5
2-Ethyl-1-butanol
Butanol
(BuOH)

Scheme 1

Supplementary Information

Figure S1: HRTEM image of Cu1.0-HT

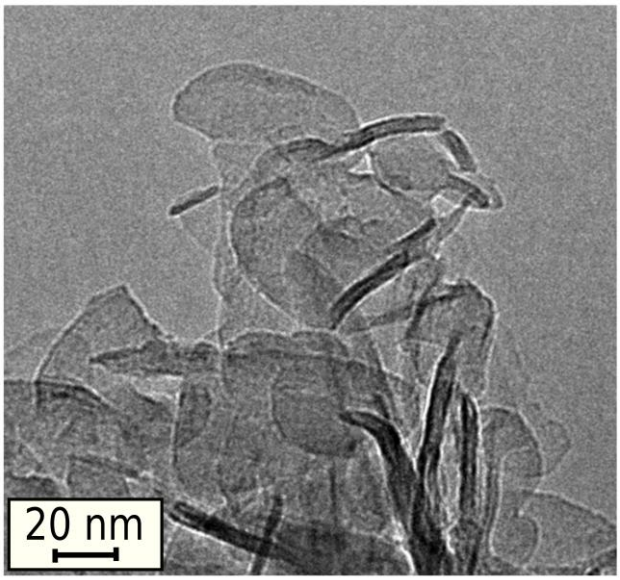

Figure S2: XPS spectra of $Cu2p_{3/2}$ core level acquired from spent Cu7.6 catalyst not pre-reduced (a) and pre-reduced (b)

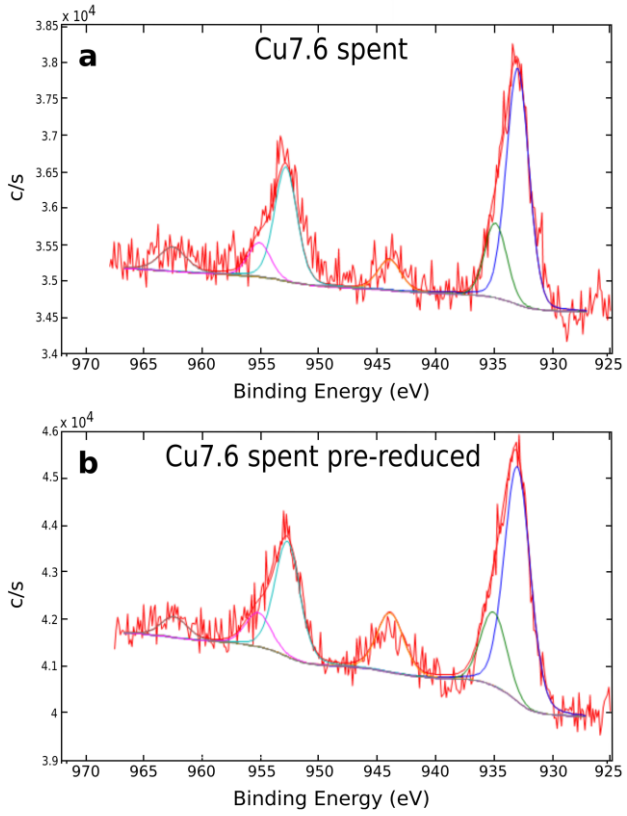

Figure S3: XPS spectra of $Cu2p_{3/2}$ core level acquired from spent Cu1.0 catalyst not pre-reduced (a) and pre-reduced (b)

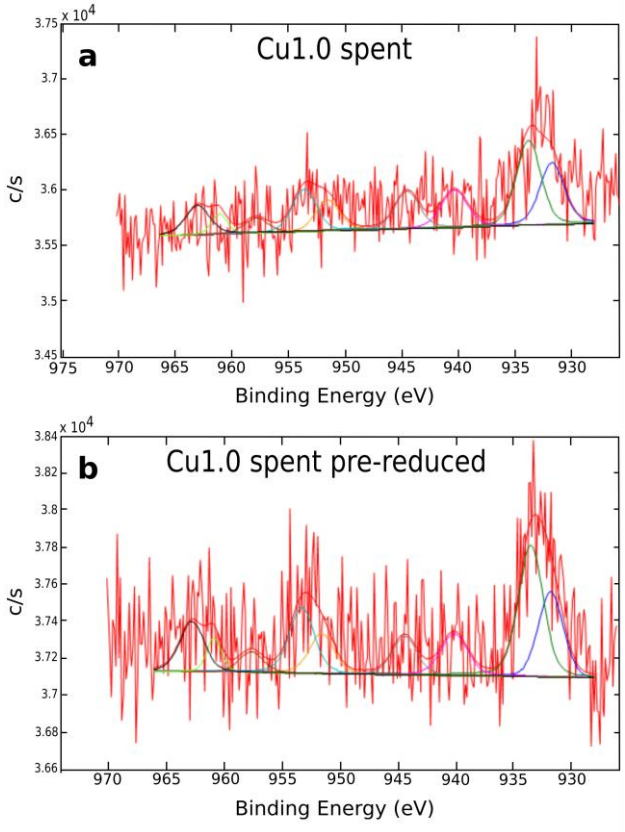

Figure S4: Diffraction pattern of Cu7.6 catalyst reduced in MeOH at 180°C under 5 MPa H_2

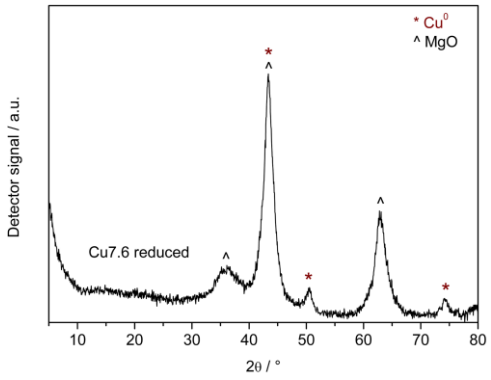

Figure S5: HRTEM characterization of Cu7.6 catalyst reduced in MeOH at 180°C under 5 MPa H_2. a: HRTEM image of a region with Cu particles in the 10-50 nm range (a1). b: HAADF/STEM image of a region with Cu particles in the 2-8 nm range (b1).